



Strong short-term non-linearity of solar irradiance fluctuations



Ata Madanchi^a, M. Absalan^a, G. Lohmann^b, M. Anvari^c, M. Reza Rahimi Tabar^{a,c,*}

^a Department of Physics, Sharif University of Technology, Tehran 11155-9161, Iran

^b Energy Meteorology Group, Institute of Physics, Carl von Ossietzky University, 26111 Oldenburg, Germany

^c Institute of Physics and ForWind, Carl von Ossietzky University, 26111 Oldenburg, Germany

ARTICLE INFO

Article history:

Received 24 November 2016

Received in revised form 31 December 2016

Accepted 4 January 2017

Keywords:

Solar energy

Intermittency

Short-time scale nonlinearity

ABSTRACT

We investigate short-term non-linearity of solar irradiance fluctuations using the multifractal detrended fluctuation analysis (MFDFA). The MFDFA shows that time series of solar irradiance have a long range correlation function with a multifractal behavior. We apply this method to solar irradiance time series from several regions around the world with resolutions of seconds and minutes. The obtained generalized Hurst and Renyi exponents $h(q)$ and $\tau(q)$ suggest the non-linear and non-stationary essence of measured irradiance time series. Also, we analyze shuffled, random phase, and rank-wised surrogated data to reveal the nature of the multifractality and conclude that linear and non-linear correlations are the dominant contributions to observed multifractal and non-linear behavior of solar irradiance.

© 2017 Elsevier Ltd. All rights reserved.

1. Introduction

The share of renewable wind and solar photovoltaic (PV) power in electricity production has constantly increased and is expected to grow further. For example, the European Union plans to generate 20% of its required electrical energy from renewables by 2020, and 60% by 2050 Schavan (2010). Recent studies on wind and solar power systems have shown that they feature strong fluctuations on different time scales, with the complexity of weather causing short-time non-Gaussian statistics in the power output of these renewable sources, see Anvari et al. (2016). These fluctuations have been characterized by Kolmogorov-like power spectra as well as q -exponential probability density functions, Anvari et al. (2016) and Rahimi Tabar et al. (2014). They complicate electrical grid operation and may endanger grid stability, Milan et al. (2013). Understanding their stochastic properties is therefore necessary for designing future power grids. It will also help to control and reduce dynamic power grid instabilities caused by renewable power production, Anvari et al. (2016) and Woyle et al. (2007).

In complex time series, two-point long-range correlations are usually characterized by scaling laws, where the scaling exponents classify the underlying processes. According to the Wiener-Khinchin theorem, the two-point correlation function $\langle x(t + \tau) \cdot x(t) \rangle$ is directly related to the power spectrum by a Fourier transform.

The correlation function is the linear regression in the $(x(t + \tau), x(t))$ plane, and it is therefore known as a linear quantity in the characterization of a given time series. There is a possibility that two completely different time series share a similar two-point correlation structure, but with different higher order stochastic properties. Therefore we need to analyze higher order (non-linear) statistical properties to fully characterize a given complex time series.

Let $\{x(t)\}$ be a given time series and consider its increment over a certain time scale τ , which is defined as $\Delta x(\tau) = x(t + \tau) - x(t)$. We denote $S(q, \tau)$ as the q th order absolute moment of $x(t)$:

$$S(q, \tau) = \langle |\Delta x(\tau)|^q \rangle. \quad (1)$$

The process is called scale invariant if the scaling behavior of the absolute moment $S(q, \tau)$ (i.e. structure function) has a power law behavior in a certain range of τ , Friedrich et al. (2011). Let us call ξ_q the exponent of the power law, i.e.

$$S(q, \tau) \simeq C_q \tau^{\xi_q} \quad (2)$$

where C_q is a prefactor. $S(q, \tau)$ is called *monofractal* (or linear) if ξ_q is a linear function of q , and *multifractal* (non-linear) if ξ_q is non-linear with respect to q . Multifractality has been introduced in the context of fully developed turbulence in order to describe the spatial fluctuations of the fluid velocity at very high Reynolds number, Peng et al. (1994). Note that this formalism may not give correct results for non-stationary time series that are affected by trends or cannot be normalized.

The simplest type of multifractal analysis (to assess linearity and non-linearity of a time series) is based on the partition

* Corresponding author at: Institute of Physics and ForWind, Carl von Ossietzky University, 26111 Oldenburg, Germany.

E-mail address: mohammed.r.rahimi.tabar@uni-oldenburg.de (M. Reza Rahimi Tabar).

function multifractal formalism, Feder (1988), Barabasi and Vicsek (1991), Peitgen et al. (1992), and Bacry et al. (2001). An improved multifractal formalism called the wavelet transform modulus maxima (WTMM) method, Muzy et al. (1991) involves tracing the maxima lines in the continuous wavelet transform over all scales. The multifractal detrended fluctuation analysis (MF-DFA) is a third method based on the identification of scaling of the q th order moments depending on the signal length. Often experimental data are affected by non-stationarities (e.g. trends), which have to be well distinguished from the intrinsic fluctuations of the system in order to find the correct scaling behavior of the fluctuations, Feder (1988), Barabasi and Vicsek (1991), Peitgen et al. (1992), Bacry et al. (2001), and Muzy et al. (1991). Fractal and multifractal analyses are widely used in social and natural sciences, Mandelbrot (1983), for instance to characterize weather conditions, Koscielny-Bunde et al. (1998), Ivanova and Ausloos (1999), and Talkner and Weber (2000), cloud shapes, Ivanova et al. (2000), geophysics, Malamud and Turcotte (1999), DNA sequences, Peng et al. (1994), Ossadnik et al. (1994), and Buldyrev et al. (1998), neuron spikes, Blesic et al. (1999) and Bahar et al. (2001), medical, physiological, and astrophysical time series, Kantelhardt (2011), as well as economic time series, Mantegna and Stanley (2000) and Liu et al. (1999).

In this paper, we address the non-linear character of solar irradiance and clear-sky index time series (i.e. irradiance normalized to clear-sky conditions) by means of the multifractal detrended fluctuation analysis (MF-DFA) using data from several regions around the world with temporal resolutions of seconds and minutes. We obtain the generalized Hurst and Renyi exponents $h(q)$ and $\tau(q)$ and show that solar irradiance time series have strong non-linear and non-stationary properties.

The paper is organized as follows. Section 2 describes and introduces the solar irradiance datasets used throughout the analyses. In Section 3, we provide a brief review of detrended fluctuation analysis (DFA) and MF-DFA methods to study scaling and multifractality of time series. MF-DFA results based on random-phase (RP) and rank-wised (RW) surrogated data are also given in this section. In Section 4, we present our results of analyzing data to probe the multifractal behavior of solar irradiance and clear-sky index and compare it to the MF-DFA results for shuffled and surrogated data sets. Section 5 contains the conclusions.

2. Description of solar irradiance data sets

Our analyses are based on large solar irradiance data sets from several countries, as summarized in Table 1. The first data set has been recorded in Hawaii using 17 horizontally oriented LI-COR LI-200 pyranometers distributed across an area of about $750 \cdot 750 \text{ m}^2$ and operating at 1 Hz between March 2010 and March 2011, Sengupta and Andreas (2010). We use both single-sensor data as well as the average of all sensors.

Also, we derive minute-averages of the single-sensor 1 Hz measurements, and use another three single-sensor data sets with the temporal resolution of minutes. Two of these data sets originate

from the global Baseline Surface Radiation Network (BSRN) BSRN (2016). They were collected in northern Spain between July 2009 and February 2013, and in Algeria (Sahara) between March 2000 and December 2013. The third minute-averaged set was recorded on the roof of the University of Oldenburg, Germany, using small ($0.242 \times 0.556 \text{ m}^2$) PV modules. It was presented in Beyer et al. (1994), and we use single-panel measurements.

Additionally, we use estimated clear-sky irradiance $I_{clearsky}$, i.e. global horizontal irradiance under a completely cloud-free atmosphere, to detrend the measured irradiance I by deriving the clear-sky index

$$k^* = \frac{I}{I_{clearsky}}. \quad (3)$$

There are different clear-sky models available, Ineichen (2006) and we use the one presented in Hammer et al. (1998) to estimate clear-sky irradiance for all the above-mentioned locations. To ensure conservative results, we only use k^* data associated with solar elevation angles greater than 10° . The clear-sky index values are positive and the maximum is around unity, except for short periods of over irradiance caused by cloud reflection, Yordanov et al. (2013).

As an example of the utilized data, Fig. 1(a) presents measured solar irradiance by a single sensor in Hawaii, where night times are removed. The corresponding clear-sky index time series is shown in panel (b), and the beginning and end of a single day are indicated by vertical lines.

3. Theory: methods of analysis

3.1. Description of methods

In this section, we review two standard methods, namely the analysis of the correlation function and the MF-DFA to investigate the fractal and multifractal properties of stochastic processes. Also, we provide details to surrogate a given time series by random-phase and rank-wised methods.

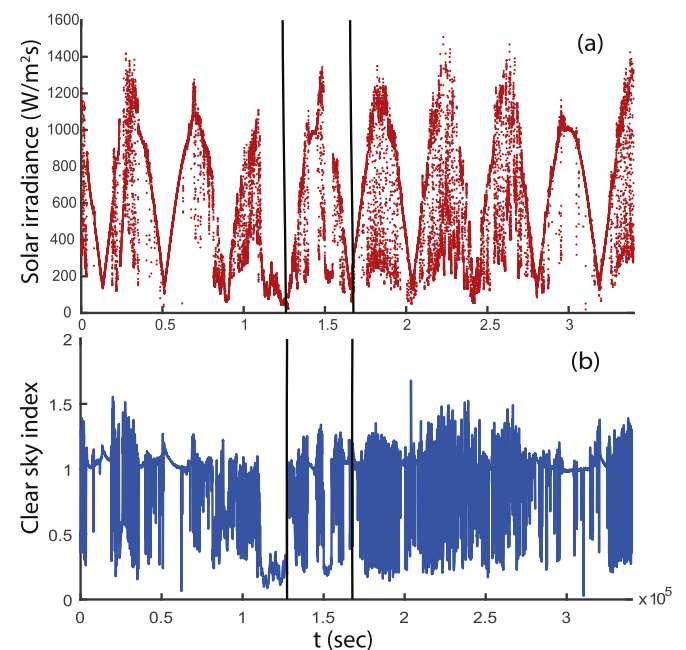


Fig. 1. (a) Measured solar irradiance of a single sensor for Hawaii and (b) its corresponding clear sky index time series. Night times have been removed.

Table 1
Data description.

| Dataset | Data points | Measurement duration (days) | Frequency (Hz) |
|------------------------------------|-------------------|-----------------------------|----------------|
| Solar irradiance, Hawaii | 14×10^6 | ~365 | 1 |
| Solar irradiance, Spain | 1.3×10^6 | ~1331 | 1/60 |
| Solar irradiance, Sahara (Algeria) | 3.7×10^6 | ~3740 | 1/60 |
| Solar irradiance, Germany | 2.7×10^5 | ~430 | 1/60 |

3.2. Long and short range correlations

Suppose a time series $x(t_i) \equiv x(i)$ for $\{i = 1, \dots, N\}$, and define the mean of x as

$$\langle x \rangle = \frac{1}{N} \sum_{i=1}^N x_i \quad (4)$$

and \bar{x}_i as

$$\bar{x}_i = x_i - \langle x \rangle. \quad (5)$$

For stationary data, the correlation function $C(s)$ is defined as

$$C(s) = \langle \bar{x}_i \bar{x}_{i+s} \rangle = \frac{1}{N-s} \sum_{i=1}^{N-s} \bar{x}_i \bar{x}_{i+s}. \quad (6)$$

If $x(i)$ is uncorrelated, $C(s)$ will be zero for $s > 0$. The short-range correlations decline exponentially [Kantelhardt \(2011\)](#),

$$C(s) \sim \exp\left(-\frac{s}{s_{max}}\right) \quad (7)$$

with a specific decay time s_{max} . For long-range correlations the decay time s_{max} increases with increasing of N , and $C(s)$ follows a power law

$$C(s) \sim s^{-\gamma} \quad (8)$$

with an exponent $0 < \gamma < 1$. The long-range correlation studied by the well-known Hurst exponent $H = 1 - \gamma/2$, [Peng et al. \(1994\)](#) and [Eke et al. \(2002\)](#) and its power spectra can be characterized by

$$S(\omega) \sim \omega^{-\beta} \quad (9)$$

with ω denoting angular frequency and the power spectrum exponent being $\beta = 2H - 1$, [Peng et al. \(1994\)](#) and [Eke et al. \(2002\)](#) for stationary data.

Non-detrending methods, like the use of correlation functions, work well if the records are long and do not involve trends. But if trends are present in the data, they might yield wrong results. In practice, almost all experimental data are affected by some non-stationarities (e.g. trends), which have to be well distinguished from the intrinsic fluctuations of the system in order to find the correct scaling behavior of the fluctuations. Detrended fluctuation analysis (DFA) is a well-established method for determining the scaling behavior of noisy data in the presence of trends without knowing a trend's origin and shape, [Xu et al. \(2005\)](#).

3.3. Detrended fluctuation analysis

The detrended fluctuation analysis (DFA) method can be used to determine scaling properties and to detect long-range correlations in non-stationary time series. The important steps of this method (see e.g. [Peng et al. \(1994\)](#), [Ossadnik et al. \(1994\)](#), [Taqqu et al. \(1995\)](#), [Hu et al. \(2001\)](#), [Chen et al. \(2002\)](#), and [Kantelhardt et al. \(2002\)](#)) are summarized as follows:

The first step is to compute the integral over the original time series $x(i)$, i.e.,

$$Y(i) = \sum_{k=1}^i x_k - \langle x \rangle \quad (10)$$

for $i = 0, \dots, N$. Then, the integrated time series is divided into N_s non-overlapping segments with length of s ($N_s = [N/s]$, where N denotes the length of the time series and $[..]$ represent the integer part of N/s). It is obvious that the divided time series will be useless for scales larger than s . In order to utilize the whole data set, the process needs to be repeated from the other side of the time series, and there will be $2N_s$ segments. Now, one can perform least square polynomial fitting of any ν th segment as P_ν . Linear, quadratic, cubic

or higher order polynomials can be used in the fitting procedure (conventionally called DFA1, DFA2, DFA3, ...), [Peng et al. \(1994\)](#), [Ossadnik et al. \(1994\)](#), and [Bunde et al. \(2000\)](#). So, for each of the segments, $Y_s(i)$ defined as

$$Y_s(i) = Y(i) - P_\nu(i). \quad (11)$$

Next, $F_s^2(\nu)$ is calculated as the fluctuation of $Y_s(i)$ as:

$$F_s^2(\nu) = \langle Y_s^2(i) \rangle = \frac{1}{s} \sum_{i=1}^s \{Y((\nu-1)s+i) - P_\nu(i)\}^2 \quad (12)$$

for each of the segment ν , $\nu = 1, \dots, N_s$. Now, $F(s)$, standard fluctuation function, is obtained by averaging over $2N_s$ segments

$$F_2(s) = \left\{ \frac{1}{2N_s} \sum_{\nu=1}^{2N_s} F_s^2(\nu) \right\}^{\frac{1}{2}} \sim s^{h(2)}. \quad (13)$$

For stationary time series, $h(2)$ is the well-known Hurst exponent H (see, e.g. [Feder \(1988\)](#)).

3.4. Multifractal detrended fluctuation analysis

The generalized fluctuation function, $F_q(s)$, is defined as

$$F_q(s) = \left\{ \frac{1}{2N_s} \sum_{\nu=1}^{2N_s} [F_s^2(\nu)]^{\frac{q}{2}} \right\}^{\frac{1}{q}} \quad (14)$$

where q can take any non-zero real value that gives the same results for $q = 2$, like standard results of DFA. For ($q = 0$), the fluctuation function should be derived by a logarithmic averaging process, because the normal averaging process in Eq. (14) causes the exponent to diverge, [Kantelhardt et al. \(2002\)](#), and

$$F_0(s) = \exp\left\{ \frac{1}{4N_s} \sum_{\nu=1}^{2N_s} \ln F_s(\nu) \right\}. \quad (15)$$

$F_q(s)$ increases with increasing scale s according to the power law

$$F_q(s) \sim s^{h(q)}, \quad (16)$$

where the function $h(q)$ is called the generalized Hurst exponent that depends on q , [Peng et al. \(1994\)](#), [Ossadnik et al. \(1994\)](#), and [Bunde et al. \(2000\)](#).

For a given q , in the linear sections of $\ln F_q(s)$ vs $\ln s$, one can estimate $h(q)$ as its slope. As mentioned in the previous subsection, for stationary processes $H = h(q = 2)$ is the Hurst exponent, and for non-stationary processes, one can show $h(q = 2) > 1.0$, [Eke et al. \(2002\)](#). In this case, the Hurst exponent can be calculated as $H = h(q = 2) - 1$, [Feder \(1988\)](#), [Bunde et al. \(2000\)](#), and [Ossadnik et al. \(1994\)](#). A scaling exponent $H = 0.5$ indicates that the time series are uncorrelated, while $0 < H < 0.5$ implies short-term anti-persistence and $0.5 < H < 1$ implies long-term persistence, [Movahed et al. \(2006\)](#). According to Eqs. (8) and (9), for non-stationary time series, the correlation exponent and power spectrum scaling are $\gamma = -2H$ and $\beta = 2H + 1$, respectively, [Peng et al. \(1994\)](#), [Ossadnik et al. \(1994\)](#), and [Eke et al. \(2002\)](#). In addition, positive values of q result in large variance (i.e., large deviations from the corresponding fit) $F_s^2(\nu)$ in Eq. (12) that affects the average $F_q(s)$ in Eq. (14). The function $h(q)$ represents the scaling behavior of the segments with large fluctuations for positive values of q . For negative values of q , small variances of $F_s^2(\nu)$ in Eq. (12) will dominate the average $F_q(s)$ in Eq. (14) and $h(q)$ describes the scaling behavior of the segments with small fluctuations, [Kantelhardt et al. \(2002\)](#).

There is a direct relationship between the generalized Hurst exponent in the MF-DFA and the classical multifractal scaling exponents $\tau(q)$ (Renyi exponent), [Kantelhardt et al. \(2002\)](#)

$$\tau(q) = qh(q) - 1. \quad (17)$$

We remind that a monofractal time series with long-range correlations is characterized by a single Hurst exponent and linear q -dependence $h(q)$. However, a multifractal time series has several Hurst exponents and a non-linear q -dependent $h(q)$. Additionally multifractal dimensions $D(q)$ are defined as

$$D(q) \equiv \frac{\tau(q)}{q-1} = \frac{qh(q) - 1}{q-1}. \quad (18)$$

The Legendre transformation from $\tau(q)$ to $f(\alpha)$ is known as the singularity spectrum, Feder (1988) and Peitgen et al. (1992) given by

$$f(\alpha) = q\alpha - \tau(q) \quad (19)$$

$$\alpha = \tau'(q) \quad (20)$$

where α is the singularity strength or Hölder exponent and $\tau'(q) = \frac{d}{dq} \tau(q)$. By using Eq. (17), one finds

$$f(\alpha) = q[\alpha - h(q)] + 1 \quad (21)$$

$$\alpha = h(q) + qh'(q). \quad (22)$$

A time series is fractal for linear $h(q)$, and multifractal for nonlinear $h(q)$. For multifractal time series, a spectrum of $f(\alpha)$ exist, Movahed et al. (2006).

3.5. Shuffled, rank-wised and random-phase surrogated data

There are two main indications for multifractality of a given time series,

1. the existence of wide or fat-tailed probability density functions, and
2. the existence of linear and non-linear correlations in the time series.

To understand the origin of multifractality one can explore each of these features separately, Manshour et al. (2015).

To destroy correlations, while maintaining the distribution's shape, a data set can be shuffled. To detect effects of fat-tailed PDFs, while keeping linear correlation, we can change the distribution of a given time series to a Gaussian distribution by performing the so called Random-Phase (RP) data surrogating. This is done simply by calculating the Fourier transform of the time series and multiplying it by random phases with a uniform distribution, Schreiber and Schmitz (1996).

Another method which changes the PDF of a time series to a Gaussian distribution is known as Rank-Wised (RW) surrogation, which keeps linear and non-linear correlations, but removes non-Gaussian distributional effects. In this method, the dependence on the fat-tailed distribution is eliminated by first ranking the N numbers in the original data, and then exchanging them rank wise by a set of N numbers from a Gaussian distribution, Bogachev et al. (2007).

4. Results

4.1. Results of MFDFA for solar irradiance

As mentioned in Section 1, solar irradiance time series are highly non-stationary and fluctuate due to different weather conditions in different time scales. By calculating $F_q(s)$, we can investigate the non-stationary behavior of solar irradiance and evaluate its scaling behavior during a day by means of a log-log plot of $F_q(s)$

vs scale s . Fig. 2 shows the results of MFDFA1 for solar irradiance measured in Hawaii with the sample rate of 1 Hz. We plotted the results for $F_q(s)$ for irradiance data measured by single sensor and averaged irradiance over an area of about $750 \times 750 \text{ m}^2$ (mean of all sensors). The analysis shows that there is a cross over time-scale $s_c \simeq 450 \text{ s} = 7.5 \text{ min}$ in the log-log plot, which divides the plots into two regions with $s > s_c$ and $s < s_c$. These kinds of regions disclose that the dominant fluctuations exhibit different correlation behaviors when varying the scale, Hu et al. (2001), Chen et al. (2002), and Kantelhardt et al. (2001). We have performed the same analysis on the clear-sky indices of single-sensor and averaged data, and present $F(s)$ versus s for $q = 2$ in Fig. 3(a). For time scales $s < s_c$ and $s > s_c$, we find the generalized Hurst exponents as $h_1(q = 2) = 1.17 \pm 0.01$ and $h_2(q = 2) = 0.93 \pm 0.02$ for single-sensor data, and $h_1(q = 2) = 1.49 \pm 0.01$ and $h_2(q = 2) = 1.03 \pm 0.03$ for averaged data, respectively, which exhibit short-term persistence of time series. Therefore one can conclude that solar irradiance and clear sky index have non-stationary ($h(q = 2) > 1$) characteristics for $s < s_c$.

To study the nonlinearity of solar irradiance in short time scales, i.e. $s < s_c$, we restrict ourselves to the region with $90 < s < 450 \text{ s}$, where $F_q(s)$ shows a clear power law behavior. For this time interval, our investigations show a strong dependence of $h(q)$ and $\tau(q)$ on q , which reveals the multifractal characteristic of solar irradiance, see Fig. 3(b) and (c).

The dependence of $h(q)$ on q leads to a non-linear relationship between $\tau(q)$ and q . A non-linear $\tau(q)$ function means multiple scaling (Evertsz and Mandelbrot, 1992; Olsson and Niemczynowicz, 1996) that is in need of hierarchy multiscaling for representing the scaling property. Fig. 3(c) represents the nonlinearity of $\tau(q)$, which can reflect the degree of multifractality. The slopes of $\tau(q)$ for irradiance and clear-sky index are measured and presented in Table 2. The slope difference between segmented fractions of the $\tau(q)$ (positive and negative q) show the degree of non-linearity. According to Fig. 3(c), the slope differences for single-sensor and mean irradiance are 2.89 and 1.30, while they amount to 1.91 and 0.93 for single-sensor and average clear-sky index. Specifically, single-sensor irradiance and clear-sky index indicate a higher degree of multifractality in their scaling property than averaged irradiance and clear-sky index. As expected, averaged time series feature smaller non-linearity in comparison to the measured time series of single sensors. In Fig. 3(d), we present the singularity spectrum ($f(\alpha)$ vs. α) of single-sensor and averaged irradiance and clear-sky index. The width of the singularity spectrum $\Delta\alpha = \alpha_{max} - \alpha_{min}$ and the range of $h(q)$ can be used to quantify the degree of multifractality Ashkenazy et al. (2003). We note that low $f(\alpha)$ values correspond to rare events (extreme values in the distribution), whereas the highest value of $f(\alpha)$ is the capacity dimension, which is obtained by assuming a uniform distribution in all the segments, Biswas et al. (2012). We find the widths of the singularity spectrum to be 3.22 ± 0.21 and 1.56 ± 0.03 for single-sensor and averaged irradiance, respectively. Therefore, we conclude that the measured irradiance from the single sensor has stronger non-linear properties than its averaged counterpart. We summarize the obtained $\Delta\alpha$ and Hurst exponents for scales $s > s_c$ ($h_1(2)$) and $s < s_c$ ($h_2(2)$) in Table 3 for both solar irradiance and clear-sky index.

4.2. Understanding the nature of multifractality

As mentioned in the methods section, by surrogating data using shuffling, random phase and rank-wised methods, we can find out which kind of multifractality exist in solar irradiance. To determine the type of multifractality, one can compare the fluctuation function for the original time series, $F_q(s)$, with the fluctuation function

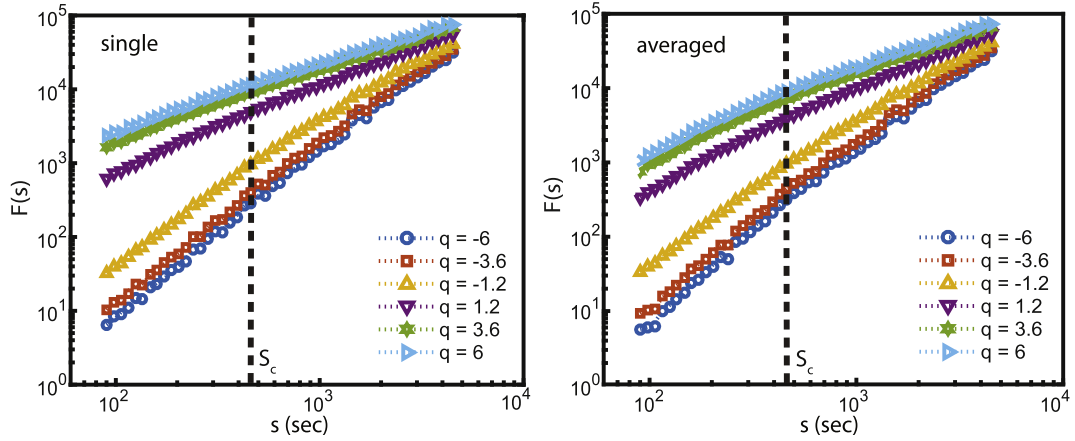


Fig. 2. F_q versus s (scale) for different values of q by multifractal detrended fluctuation analysis for single sensor data and the average of all sensors in the field.

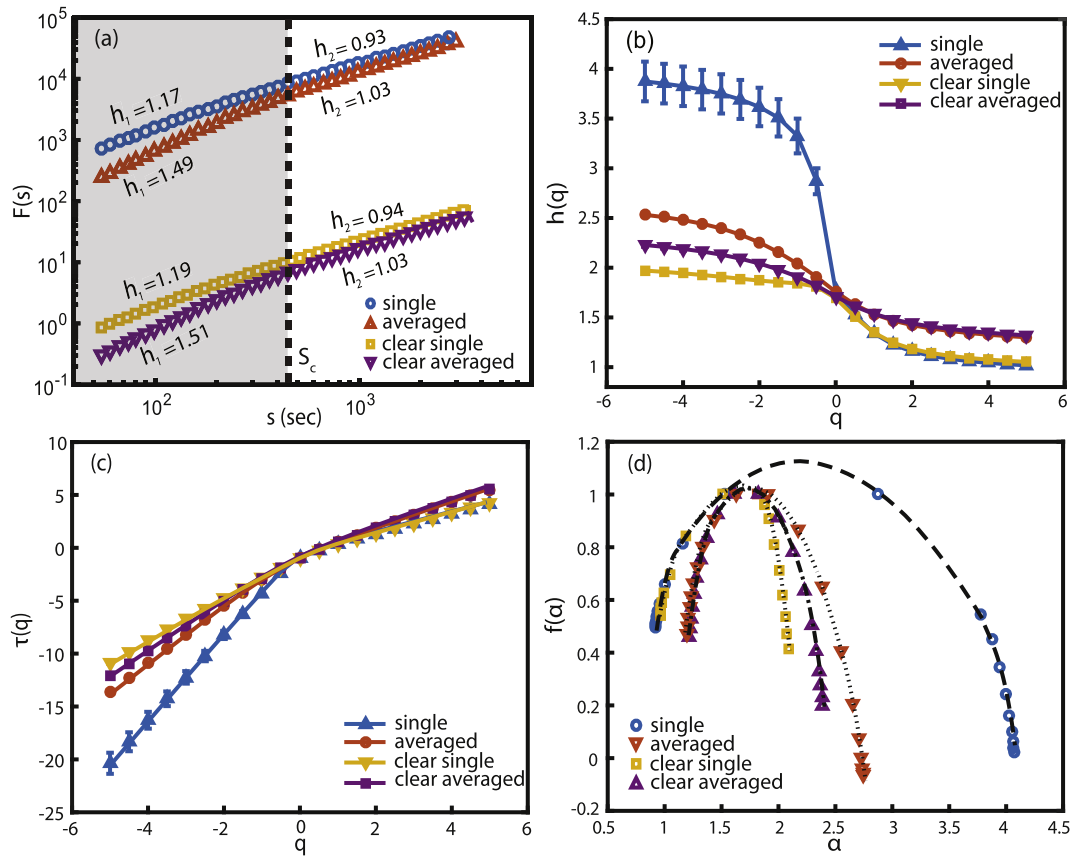


Fig. 3. (a) Fluctuation function $F_{q-2}(s)$ versus scale s , (b) multifractal scaling exponent $h(q)$ versus q , (c) classical multifractal scaling exponent, $\tau(q)$ versus q . The region with $q > 0$ has a different slop than the region $q < 0$ for each data set. (d) Singularity spectrum $f(\alpha)$, which shows multifractal characteristics of different strengths for single-sensor and mean irradiance and clear-sky index data by comparing the widths of α .

for the shuffled, random phase and rank-wise surrogated data, i.e., $F_q^{shuf}(s)$, $F_q^{RP-sur}(s)$ and $F_q^{RW-sur}(s)$, respectively. By considering their ratio we have:

$$F_q(s)/F_q^{shuf}(s) = s^{h(q)-h_{shuf}(q)} = s^{h_{corr}(q)}, \quad (23)$$

$$F_q(s)/F_q^{RP-sur}(s) = s^{h(q)-h_{RP-sur}(q)} = s^{h_{PDF-RP}(q)} \quad (24)$$

$$F_q(s)/F_q^{RW-sur}(s) = s^{h(q)-h_{RW-sur}(q)} = s^{h_{PDF-RW}(q)}. \quad (25)$$

Table 2
Slope of the Renyi exponent $\tau(q)$ for irradiance and clear-sky index data.

| Data | Slope | |
|---------------------------|--------------|-------------|
| | $-6 < q < 0$ | $0 < q < 6$ |
| Irradiance, single | 3.99 | 1.11 |
| Irradiance, averaged | 2.63 | 1.33 |
| Clear-sky index, single | 1.99 | 1.08 |
| Clear-sky index, averaged | 2.28 | 1.35 |

Multifractality of a time series can be attributed to three causes. The first is a broad probability density function (PDF) of the time series, the second is a linear correlation inherit in the data, and the third is the presence of mixed linear and non-linear correlations. In Fig. 4, we present the results of these analyses for single-sensor and averaged irradiance.

Table 3
Numerical results of MF-DFA for single-sensor and averaged irradiance and clear-sky index data.

| Data | $h_1(2) (s < s_c)$ | $h_2(2)(s > s_c)$ | $\tau(q = 2)$ | $\Delta\alpha$ |
|---------------------------|--------------------|-------------------|-----------------|-----------------|
| Irradiance, single | 1.17 ± 0.01 | 0.93 ± 0.02 | 1.31 ± 0.02 | 3.22 ± 0.21 |
| Irradiance, averaged | 1.49 ± 0.01 | 1.03 ± 0.03 | 1.84 ± 0.02 | 1.56 ± 0.03 |
| Clear-sky index, single | 1.19 ± 0.01 | 0.94 ± 0.01 | 1.36 ± 0.01 | 1.17 ± 0.02 |
| Clear-sky index, averaged | 1.51 ± 0.01 | 1.03 ± 0.01 | 1.88 ± 0.01 | 1.18 ± 0.02 |

The shuffled time series always has a fractal behavior with $h_{\text{shuf}}(q) = 0.5$. As shown in Fig. 4a and c, there are big differences between the original $h(q)$ and $h_{\text{shuf}}(q)$ for single-sensor and averaged irradiance measurements. This indicates that the correlation (linear and non-linear) is the origin of multifractality. The multifractal exponents of the rank-wised surrogated data are closest to the original $h(q)$, while the random phase surrogated data lies between the two cases. We can conclude that both linear and non-linear correlations are responsible for the observed multifractality of solar irradiance time series. Table 4 shows the generalized Hurst exponent and width of the singularity spectrum for the

original and the random phase and rank wised surrogated time series. Tables 5 and 6 show the values of the Hurst exponent H , the power spectrum exponent β and the autocorrelation exponent γ , for the irradiance data measured by a single sensor as well as that averaged over all sensors in the field.

4.3. Multifractality of solar irradiance for different countries

We repeat our analysis presented in Section 4 for solar irradiance measured in Algeria, Germany, Hawaii and Spain to investigate the scaling and multifractal behaviors in different locations.

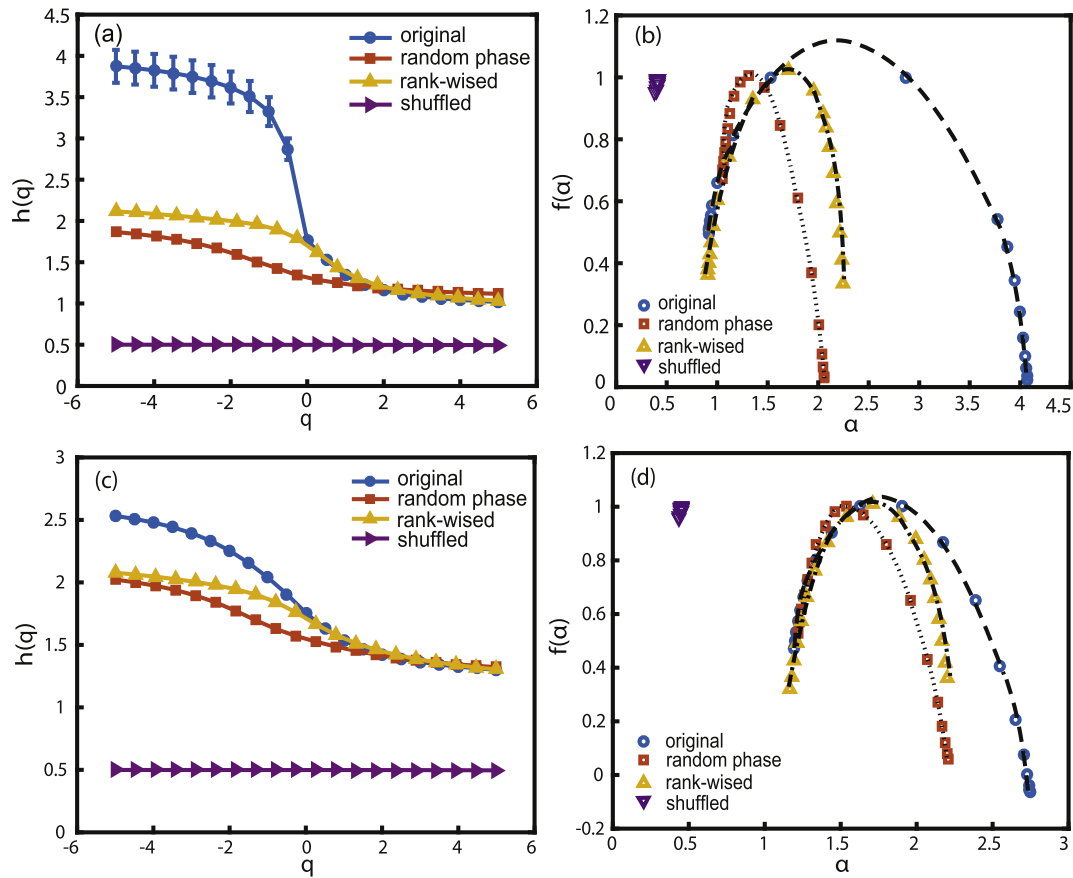


Fig. 4. (a) Multifractal exponents of irradiance time series measured by a single sensor, calculated from random phase, rank-wised surrogated and shuffled time series, as well as results for the original data. (b) Singularity spectrum for single-sensor data, where the width of $f(\alpha)$ is a measure of multifractality. (c) Hurst exponent for averaged irradiance time series and (d) its singularity spectrum.

Table 4
Generalized Hurst exponent, $h(q = 2)$ and $\Delta\alpha$ for the irradiance data measured by a single sensor and that averaged over all sensors in the field.

| Single sensor | $h(q = 2)$ | $\Delta\alpha$ | Averaged | $h(q = 2)$ | $\Delta\alpha$ |
|---------------|-----------------|----------------|--------------|-----------------|----------------|
| Original | 1.17 ± 0.01 | 3.22 | Original | 1.49 ± 0.01 | 1.56 |
| Random phase | 1.18 ± 0.01 | 1.01 | Random phase | 1.42 ± 0.01 | 0.99 |
| Rank-wised | 1.21 ± 0.01 | 1.34 | Rank-wised | 1.46 ± 0.01 | 1.03 |
| Shuffled | 0.49 ± 0.01 | 0.01 | Shuffled | 0.49 ± 0.02 | 0.01 |

Table 5

The Hurst exponent H , spectrum exponent γ and correlation exponent β , for data measured by a single sensor.

| Single sensor | H | γ | β |
|---------------|-----------------|------------------|-----------------|
| Original | 0.17 ± 0.01 | -0.34 ± 0.01 | 1.34 ± 0.01 |
| Random phase | 0.18 ± 0.01 | -0.36 ± 0.01 | 1.36 ± 0.01 |
| Rank-wised | 0.21 ± 0.01 | -0.42 ± 0.01 | 1.42 ± 0.01 |
| Shuffled | 0.51 ± 0.01 | N.A. | N.A. |

Table 6

The Hurst exponent H , spectrum exponent γ and correlation exponent β , for averaged data in the field.

| Averaged | H | γ | β |
|--------------|-----------------|------------------|-----------------|
| Original | 0.49 ± 0.01 | -0.98 ± 0.01 | 1.98 ± 0.01 |
| Random phase | 0.42 ± 0.01 | -0.84 ± 0.01 | 1.84 ± 0.01 |
| Rank-wised | 0.46 ± 0.01 | -0.92 ± 0.01 | 1.92 ± 0.01 |
| Shuffled | 0.49 ± 0.01 | N.A. | N.A. |

The sample rate of the used data is 1/60 Hz and we use about 300 days from each data set. Fig. 5 shows the results of MF-DFA for all data sets of these countries. The plot of $F(s)$ versus s in Fig. 5a indicates that the countries share two common crossover time scales located at $s_{1c} \approx 7$ min and $s_{2c} \approx 90$ min. In Section 4. A, we had also observed $s_{1c} \approx 7$ min for the analysis of 1 Hz data. The multifractal characteristics of solar irradiance for time scales $s < s_{1c}$ have been discussed in Section 4.1 (with resolutions of seconds). In this section we restrict ourselves to time scales in the interval $s_{1c} < s < s_{2c}$. As shown in Fig. 5(a), we find a non-stationary behavior for this interval (i.e. $h_1 > 1$), however with

Table 7

Slope of the mass exponent functions $\tau(q)$ of solar irradiance data for different countries and locations.

| Data | Slope | |
|---------|---------------|--------------|
| | $-10 < q < 0$ | $0 < q < 10$ |
| Algeria | 2.24 | 1.38 |
| Hawaii | 2.54 | 0.86 |
| Spain | 2.39 | 1.11 |
| Germany | 2.42 | 0.94 |

slight changes in the slope of $F(s)$ (generalized Hurst exponent) for different countries. In this respect, Germany exhibits the longest correlated irradiance fluctuations, followed by Algeria, Spain and Hawaii.

In panels (b), (c), and (d) of Fig. 5, all data sets are shown to have a strong multifractal nature as expressed by the q dependence of $h(q)$ and $\tau(q)$, as well as the singularity spectrum $f(\alpha)$. The slopes of $\tau(q)$ are summarized for the irradiance measured in different countries and locations in Table 7. Accordingly, the degree of non-linearity is quantified by the slope difference between segmented fractions of $\tau(q)$. The slope difference for Algeria, Hawaii, Spain and Germany are 0.86, 1.68, 1.28 and 1.48, respectively. The obtained results indicate that the irradiance data measured in Hawaii and Germany possess a higher degree of multifractality, see Fig. 5(c). In Fig. 5(d), the widths of the singularity spectra are 1.05 ± 0.03 , 1.82 ± 0.03 , 1.42 ± 0.03 and 1.63 ± 0.05 for Algeria, Hawaii, Spain and Germany, respectively. The data from Hawaii consistently exhibits the strongest indications of multifractality, followed by Germany, Spain, and Algeria.

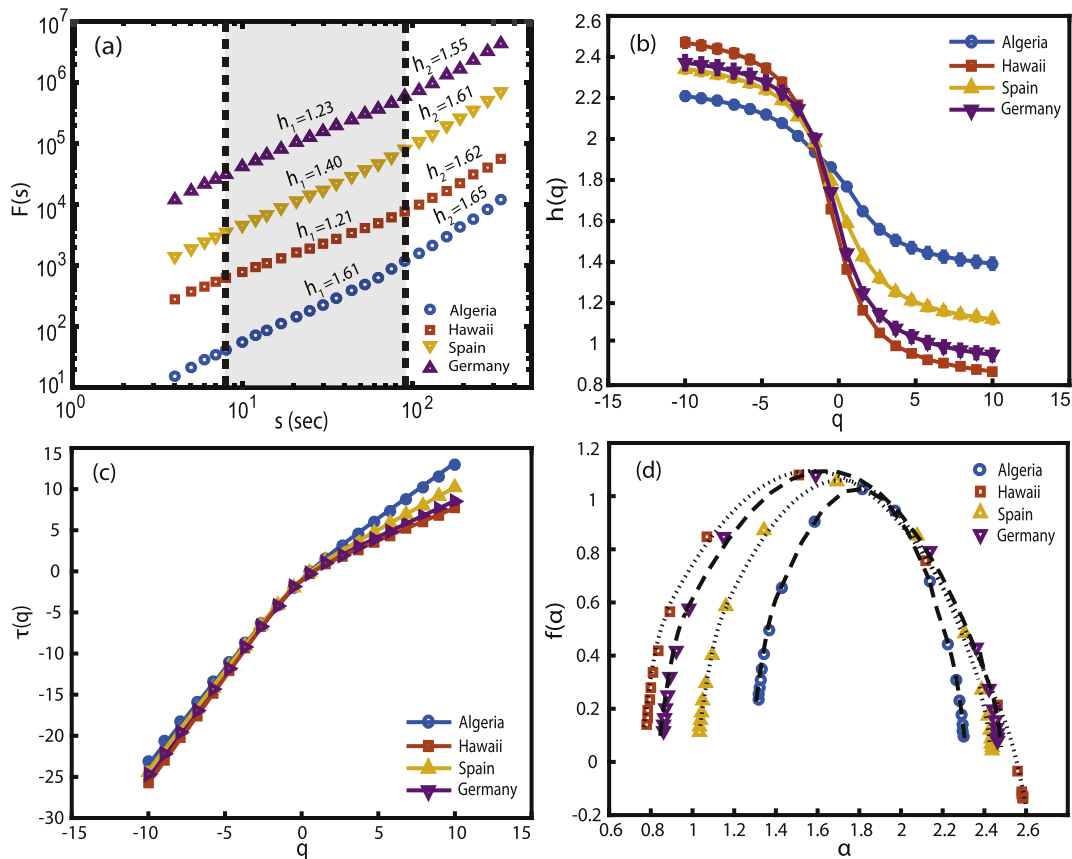


Fig. 5. (a) Standard fluctuation functions versus scale demonstrate two crossover scales, s_{1c} and s_{2c} in four countries. (b) Multifractal scaling exponent $h(q)$ and (c) classical multifractal scaling exponent $\tau(q)$. (d) Singularity spectrum $f(\alpha)$ shows that measurements in different countries demonstrate different multifractal strength. Multifractality of the irradiance time series is strongest for Hawaii and decreases for Germany, Spain and Algeria (in that order).

Table 8

Numerical results of the generalized Hurst exponent and singularity spectrum width, $\Delta\alpha$.

| Location | $h(q = 2)$ | $\Delta\alpha$ |
|----------|-----------------|-----------------|
| Algeria | 1.61 ± 0.02 | 1.05 ± 0.03 |
| Hawaii | 1.21 ± 0.02 | 1.82 ± 0.03 |
| Spain | 1.40 ± 0.01 | 1.42 ± 0.03 |
| Germany | 1.23 ± 0.02 | 1.63 ± 0.05 |

For the above mentioned reasons, we can conclude that nonlinear aspects of solar irradiance are dependent on the geographic and weather conditions, see Table 8.

5. Conclusion

In this paper, we studied the multifractal behavior of solar irradiance using the MF-DFA method. By analyzing extensive experimental data for solar irradiance from several regions around the world with resolutions of seconds and minutes, we show that there are two crossover time scales (7.5 min and 90 min) on the scaling behavior of standard fluctuation functions versus scale. Analyzing the shuffled, random phase and rank wise surrogated data suggests that the multifractal nature of solar irradiance is due to the linear and nonlinear correlations, while the width of the probability density function does not play an important role. We find that irradiance data from different countries and locations show non-stationary fluctuations, with multifractality being strongest for the measurements from Hawaii and weakest for those from Algeria. The former location is well known for almost omnipresent cumulus clouds Hinkelman (2013), while the latter is dominated by desert-type conditions. The degree of multifractality can thus be considered a direct consequence of the frequency with which broken clouds occur. Our findings contribute to a better understanding of solar irradiance fluctuations. Reconstruction of multifractal irradiance time series Muzy et al. (1991) and study the power grid performance with multifractal feed-in are the next steps of this work, where recently have been considered by some researchers Mitra et al. (2016) and Schmietendorf et al. (2016).

Acknowledgments

This work was partially supported by Sharif University of Technology's Office of Vice President for Research under Grant No. G930209. We acknowledge the National Renewable Energy Laboratory in the United States for providing the data in Hawaii. BSRN data was kindly made available by the World Radiation Monitoring Center (WRMC) and we particularly acknowledge Mohamed Mimouni and Xabier Olano, Managers of BSRN stations of Tamanrasset (Algeria) and Cener (Spain), respectively.

References

Anvari, M., Lohmann, G., Wächter, M., Milan, P., Lorenz, E., Heinemann, D., Rahimi Tabar, M.R., Peinke, J., 2016. Short term fluctuations of the wind and solar power systems. *New J. Phys.* 18, 063027.

Ashkenazy, Y., Baker, D.R., Gildor, H., Havlin, S., 2003. Nonlinearity and multifractality of climate change in the past 420,000 years. *Geophys. Res. Lett.* 30, 2146.

Bacry, E., Delour, J., Muzy, J., 2001. Multifractal random walk. *Phys. Rev. E* 64, 026103.

Bahar, S., Kantelhardt, J.W., Neiman, A., Rego, H.H.A., Russell, D.F., Wilkens, L., Bunde, A., Moss, F., 2001. Long range temporal anticorrelations in paddlefish electro-receptors. *Europhys. Lett.* 56, 454.

Barabasi, A., Vicsek, T., 1991. Multifractality of self-affine fractals. *Phys. Rev. A* 44, 2730.

Beyer, H.G., Hammer, A., Luther, J., Poplawski, J., Stolzenburg, K., Wieting, P., 1994. Analysis and synthesis of cloud pattern for radiation field studies. *Solar Energy* 52, 379.

Biswas, A., Zeleke, T.B., Si, B.C., 2012. Multifractal detrended fluctuation analysis in examining scaling properties of the spatial patterns of soil water storage. *Nonlin. Processes Geophys.* 19, 227.

Blesic, S., Milosevic, S., Stratimirovic, D.J., Ljubisavljevic, M., 1999. Detrended fluctuation analysis of time series of a firing fusimotor neuron. *Physica A* 268, 275.

Bogachev, M.I., Eichner, J.F., Bunde, A., 2007. Effect of nonlinear correlations on the statistics of return intervals in multifractal data sets. *Phys. Rev. Lett.* 99, 240601.

BSRN, 2016. The Data Sets are Available at <ftp://ftp.bsrn.awi.de/>, see also <http://bsrn.awi.de/data/data-retrieval-via-ftp.html>.

Buldyrev, S.V., Dokholyan, N.V., Goldberger, A.L., Havlin, S., Peng, C.K., Stanley, H.E., Viswanathan, G.M., 1998. Analysis of DNA sequences using methods of statistical physics. *Physica A* 249, 430.

Bunde, A., Havlin, S., Kantelhardt, J.W., Penzel, T., Peter, J.H., Voigt, K., 2000. Correlated and uncorrelated regions in heart-rate fluctuations during sleep. *Phys. Rev. Lett.* 85, 3736.

Chen, Z., Ivanov, P. Ch., Hu, K., Stanley, H.E., 2002. Effect of nonstationarities on detrended fluctuation analysis. *Phys. Rev. E* 65, 041107.

Eke, A., Herman, P., Kocsis, L., Kozak, L.R., 2002. Fractal characterization of complexity in temporal physiological signals. *Physiol. Meas.* 23, R1–R8.

Evertsz, C.J.G., Mandelbrot, B.B., 1992. Multifractal measures. In: Peitgen, H.-O. et al. (Eds.), *Chaos and fractals. New frontiers of science.* Springer-Verlag, New York, NY, pp. 921–953.

Feder, J., 1988. *Fractals.* Plenum Press, New York.

Friedrich, R., Peinke, J., Sahimi, M., Rahimi Tabar, M.R., 2011. Approaching complexity by stochastic methods: from biological systems to turbulence. *Phys. Rep.* 506, 87.

Hammer, A., Heinemann, D., Westerhellweg, A., Beyer, H.G., Reise, C., 1998. Daylight and solar irradiance data derived from satellite observations – The Satellight Project. In: 9th Conf. on Satellite Meteorology and Oceanography No. 2.

Hu, K., Ivanov, P. Ch., Chen, Z., Carpena, P., Stanley, H.E., 2001. Effect of trends on detrended fluctuation analysis. *Phys. Rev. E* 64, 011114.

Ivanova, K., Ausloos, M., 1999. Application of the detrended fluctuation analysis (DFA) method for describing cloud breaking. *Physica A* 274, 349.

Ivanova, K., Ausloos, M., Clothiaux, E.E., Ackerman, T.P., 2000. Break-up of stratus cloud structure predicted from non-Brownian motion liquid water and brightness temperature fluctuations. *Europhys. Lett.* 52, 40.

Ineichen, P., 2006. Comparison of eight clear sky broadband model against 16 independent data banks. *Solar Energy* 80, 468.

Kantelhardt, J.W., 2011. *Mathematics of Complexity and Dynamical Systems.* Springer, New York, pp. 463–387.

Kantelhardt, J.W., Koscielny-Bunde, E., Rego, H.H.A., Havlin, S., Bunde, A., 2001. Detecting long-range correlations with detrended fluctuation analysis. *Physica A* 295, 441–454.

Kantelhardt, J.W., Zschiegner, S.A., Koscielny-Bunde, E., Havlin, S., Bunde, A., Stanley, H.E., 2002. Multifractal detrended fluctuation analysis of nonstationary time series. *Physica A* 316, 87.

Koscielny-Bunde, E., Bunde, A., Havlin, S., Roman, H.E., Goldreich, Y., Schellnhuber, H.-J., 1998. Indication of a universal persistence law governing atmospheric variability. *Phys. Rev. Lett.* 81, 729.

Liu, Y., Gopikrishnan, P., Cizeau, P., Meyer, M., Peng, C.K., Stanley, H.E., 1999. *Phys. Rev. E* 60, 1390.

Malamud, B.D., Turcotte, D.L., 1999. Self-affine time series: measures of weak and strong persistence. *J. Stat. Plan. Infer.* 80, 173.

Mandelbrot, B.B., 1983. *The Fractal Geometry of Nature.* W.H. Freeman, New York.

Manshour, P., Rahimi Tabar, M.R., Peinke, J., 2015. Fully developed turbulence in the view of horizontal visibility graphs. *J. Stat. Mech.*, P08031.

Mantegna, R.N., Stanley, H.E., 2000. *An Introduction to Econophysics.* Cambridge University Press, Cambridge.

Milan, P., Wächter, M., Peinke, J., 2013. Turbulent character of wind energy. *Phys. Rev. Lett.* 110, 138701.

Mitra, C., Choudhary, A., Sinha, S., Kurths, J., Donner, R.V., 2016. Multi-Node Basin Stability in Complex Dynamical Networks. [arXiv:1612.06015](https://arxiv.org/abs/1612.06015).

Movahed, M.S., Jafari, G., Ghasemi, F., Rahvar, S., Rahimi Tabar, M.R., 2006. Multifractal detrended fluctuation analysis of sunspot time series. *J. Stat. Mech. Theory, P02003*.

Muzy, J., Bacry, E., Arneodo, A., 1991. Wavelets and multifractal formalism for singular signals: application to turbulence data. *Phys. Rev. Lett.* 67, 3515.

Ossadnik, S.M., Buldyrev, S.B., Goldberger, A.L., Havlin, S., Mantegna, R.N., Peng, C.K., Simons, M., Stanley, H.E., 1994. Correlation approach to identify coding regions in DNA sequences. *Biophys. J.* 67, 64.

Peitgen, H.O., Jurgens, H., Saupe, D., 1992. *Chaos And Fractals.* Springer-Verlag, New York.

Peng, C.K., Buldyrev, S.V., Havlin, S., Simons, M., Stanley, H.E., Goldberger, A.L., 1994. Mosaic organization of DNA nucleotides. *Phys. Rev. E* 49, 1685.

Rahimi Tabar, M.R., Anvari, M., Lohmann, G., Heinemann, D., Wächter, M., Milan, P., Lorenz, E., Peinke, J., 2014. Kolmogorov spectrum of renewable wind and solar power fluctuations. *Eur. Phys. J. Special Topics* 223, 2637.

Schavan, A., 2010. Germany's energy research plan. *Science* 330, 295.

Schmietendorf, K., Peinke, J., Kamps, O., 2016. On the Stability and Quality of Power Grids Subjected to Intermittent Feed-In. [arXiv:1611.08235](https://arxiv.org/abs/1611.08235).

Schreiber, T., Schmitz, A., 1996. Improved surrogate data for nonlinearity tests. *Phys. Rev. Lett.* 77, 635.

Sengupta, M., Andreas, A., 2010. Oahu Solar Measurement Grid (1-Year Archive): 1-Second Solar Irradiance; Oahu, Hawaii (Data); NREL Report No. DA-5500-56506.

- Taqqu, M.S., Teverovsky, V., Willinger, W., 1995. Estimators for long-range dependence: an empirical study. *Fractals* 3, 785.
- Talkner, P., Weber, R.O., 2000. Power spectrum and detrended fluctuation analysis: application to daily temperatures. *Phys. Rev. E* 62, 150.
- Woyte, A., Belmans, R., Nijs, J., 2007. Fluctuations in instantaneous clearness index: analysis and statistics. *Solar Energy* 81, 195.
- Xu, L., Ivanov, P. Ch., Hu, K., Chen, Z., Carbone, A., Stanley, H.E., 2005. Quantifying signals with power-law correlations: a comparative study of detrended fluctuation analysis and detrended moving average techniques. *Phys. Rev. E* 71, 051101.
- Yordanov, G.H., Midtgard, O.M., Saetre, T.O., Nielsen, H.K., Norum, L.E., 2013. Overirradiance (cloud enhancement) events at high latitudes. *IEEE J. Photovoltaics* 3, 271.
- Hinkelman, L.M., 2013. Differences between along-wind and cross-wind solar irradiance variability on small spatial scales. *Solar Energy* 88, 192–203. <http://dx.doi.org/10.1016/j.solener.2012.11.011>.